Diamond & Related Materials 141 (2024) 110680

Contents lists available at ScienceDirect

Diamond & Related Materials

journal homepage: www.elsevier.com/locate/diamond

# Graphene nanoplatelets anchored into Ag doped spinel $CoFe_2O_4$ nanohybrid: Synthesis, structural, electrical, superior dielectric and room temperature induced ferromagnetism performance for high frequency device application

Krutika L. Routray, Sunirmal Saha *

*Department of Physics, C.V. Raman Global University, India*

ARTICLE INFO

*Keywords:*
Graphene
Impedance study
Nanocomposites
Magnetism
Structural

ABSTRACT

Graphene (GnPs) incorporated Ag-$CoFe_2O_4$ nanocomposite was synthesized using a simple solvothermal method using green synthesis method by okra plant extract. The prepared materials were micro-analyzed by X-ray diffraction (XRD) measurements, Fourier transform-infrared (FT-IR) spectra, Field emission scanning electron microscope (FESEM) and transmission electron microscopy (TEM) microanalysis. The average particle size obtained from XRD data was calculated to be 32.6 nm for Ag- CFO nanoparticles and 24 nm for GnPs doped Ag-CFO nanocomposite which was in good agreement with the particle size (in nm) estimated from the FESEM and TEM micrographs. The effective charge carriers transfer from the from Ag- CFO nanoferrites to graphene pallets and in case of GnPs incorporated Ag- CFO nanocomposite and the long-drawn-out recombination of electron–hole pairs were evidently shown by means of room temperature PL measurements. The photocurrent values well support the PL measurements signifying transfer of the electron-hole pairs. Light dependent Electrochemical Impedance Spectroscopy indicates the incidence of a light dependent dielectric relaxation phenomenon. Massive dielectric values with low loss suggest the GnPs doped nanohybrid to be well suited for high frequency device application. Interestingly, incorporation of GnPs alters the electronic configuration of the nanocomposites inducing ferromagnetic interaction.

## 1. Introduction

Spinel ferrites have demonstrated significant potential in various applications such as in storage media, gas sensing, ferro-fluids, microelectronics, microwave devices and recently in medicine owing to their flexible structure, high electrical resistance, tunable composition, high chemical and thermal stability, high permeability, and significant mechanical properties [1–6]. Interest in ferrites have gathered among researchers these days because of their resistivity which is approximately ten times higher than pure iron making them preferable for high frequency devices and applications [7]. Extensive research is being carried out to improve the properties of nanoferrites to expand their application in modern life applications. Among the spinel ferrites, cobalt ferrite ($CoFe_2O_4$, CFO) is a known ferromagnetic material and plays significant role as a consequence of its exceptional properties [5–8]. It is comprised of spinel structure (inverse) where $Fe^{3+}$ ions occupy the tetrahedral (A) sites and $Fe^{2+}$ and $Co^{2+}$ ions occupy the octahedral (B) sites [8,9]. CFO is observed to have outstanding magnetic and electrical properties, high porosity, high value of saturation magnetic flux density, high immersion polarization, low coercivity, high permittivity and permeability and appreciable resistivity [8–11].

Considering the literature in view, CFO is preferred to dope with transition metals to enhance the scope of these materials for various aforementioned applications [10,12]. Doping in ferrites modify the cation distribution and lead to noticeable changes in the structural, magnetic, and electrical properties [12–14]. Despite our foregoing efforts related to the development of metal-doped $MFe_2O_4$ (M = Co, Ni, Zn, etc.), there still exists significant knowledge gaps concerning the ideal choice for selecting metal dopants and in addition to gain insight into the redox reaction and metal complexation occurring through the catalytic process [15–17]. Ag metal is highly stable and has proven to have extraordinary electrical as well as thermal conductivity. Hence,

* Corresponding author.
*E-mail address:* sunirmal.saha@cgu-odisha.ac.in (S. Saha).

https://doi.org/10.1016/j.diamond.2023.110680
Received 25 July 2023; Received in revised form 23 October 2023; Accepted 25 November 2023
Available online 30 November 2023

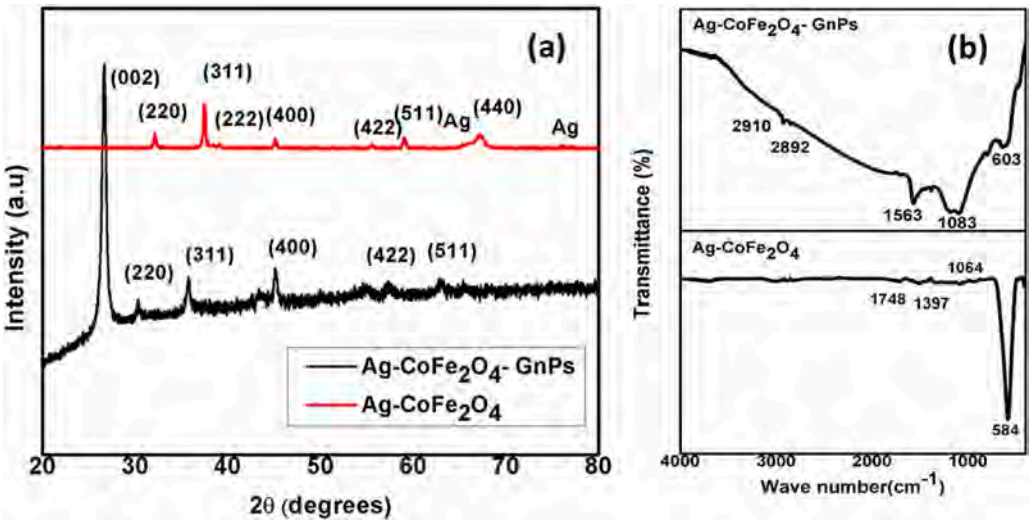


**Fig. 1.** (a) XRD pattern (b) FT-IR spectra of Ag- $CoFe_2O_4$ nanoparticles and GnPs doped Ag- $CoFe_2O_4$ nanocomposites.

doping of Ag with CFO makes it a potentially promising dopant to improve the nanoferrites for various applications. Mahajan et al. and Satheeshkumar et al. reported on the antibacterial activity of ag doped CFO and proposed a modified mechanism of action for the antibacterial activity. M. Kaiser suggested that the Ag doped CFO materials can be recommended for fabrication of exchange spring magnets and electrode materials [17–21]. In our previous work, it was found that Ag doped in CFO divulges excellent dielectric and magnetic properties with low loss values [18–21]. Furthermore, the properties of these transition metal doped ferrites can be enhanced by creating their composites [22]. Various 2D nanomaterials such as graphene, hexagonal boron nitride (hBN,) transition metal nitride or carbide (MXene) are used in synthesizing nano ferrite composites. Dong et al. reported an review on graphene-derived e.g. graphene and graphene oxide materials incorporated with 2D materials (e.g. hBN, $MoS_2$, $Ti_3C_2T_x$) for the reinforcement of epoxy resins. Cai et al. worked on the progress of 2D nanomaterials with graphene for enhancement in applications related to fire safety of polymer (nano) composites. Ramezani et al. reported on the Multi-walled carbon nanotube grafted with 2, 6-bis[2-(amino methyl) phenol]pyridine (BAPP) synthetic ligands for electrode applications [23–25]. Graphene is known to have excellent mechanical and electrical properties owing to its large surface area, unique thermal stability and minimal dielectric loss, leasing to an exceptional material for synthesizing hybrids or composites [24–26].

Several methods are engaged in preparing nano ferrites composites namely solid-state reaction, co-precipitation, sol-gel auto combustion technique, hydrothermal processes, micro-emulsion, mechanochemical alloying, electro-spinning, self-combustion, citrate/oxalate precursor and spray drying [27–30]. Researchers are currently interested in reducing the toxic effect of chemical on environment by employing noble synthesis techniques known as green chemistry, among which the most focused area of synthesis is by using plant and natural resources. As a result, the synthesized nano ferrite composites display less toxicity and more biocompatibility. Moreover, owing to the present scenario of environmental complications and pollution arising due to chemical synthesis, synthesis using green chemistry provides an alternative advancement in diverse applications. Adil et al. discussed the biogenic synthesis of metallic nanoparticles to manage the potential environmental impacts from conventional synthesis [31]. Similar work has been reported by Benakashani et al., Routray et al. and Behzadi et al. regarding green synthesis of nanoparticles using root and leaf extract [32–34]. Ahmadian-Fard-Fini et al. successfully synthesized $Fe_3O_4$-carbon dots by lemon and grapefruit extracts to be used in photoluminescence sensor for detecting *E. coli* bacteria. They also reported on synthesis of magnetic hollow $NiFe_2O_4$-carbon dots nanocomposite material [35–36].

Herein, graphene (GnPs) incorporated Ag doped CFO nanocomposites are prepared by facile solvothermal method using okra plant extract as a fuel against high frequency devices application. By mixing Ag-doped cobalt ferrite, and graphene, the authors are aiming to create a composite material with enhanced properties that are not achievable with any single material. These enhanced properties are related to optical, electrical, magnetic, and dielectric characteristics. Combining these materials might allow for the fine-tuning of certain properties. For example, graphene is known for its electrical conductivity, while cobalt ferrite can have magnetic properties. The addition of silver (Ag) might introduce new functionalities or enhance existing ones. Herein, graphene (GnPs) incorporated Ag doped CFO nanocomposites are prepared by facile solvothermal method using okra plant extract as a fuel against high frequency devices application. We developed a novel green synthesis method for creating this composite material, that could be considered an innovative aspect and gives enhanced properties. The key aim of this research is to use an eco-friendly, low-cost method for green synthesis of nanocomposite.

## 2. Experimental details

Ag-CFO was synthesized via. okra extract assisted green synthesis technique as described elsewhere [17]. GnPs was purchased from Nanopar Tech, India. GnPs-Ag-CFO nanocomposite was synthesized using ultra-sonication method. In this process, 91 wt% of prepared nano Ag-CFO particles and 9 wt% mg GnPs was put together in 300 mL of distilled $H_2O$ and ultra-sonicated for 2 h to produce a homogeneous solution. This obtained solution was then transferred to an oven and heated at 80 °C for 6 h and subsequently cooled down. Lastly, the final obtained black precipitate mixture was ground thoroughly to form powder.

Structural characterizations have been done by qualitative XRD (Rigaku Ultima-IV X-ray diffractometer) at room temperature and FTIR-Shimadzu-8000 spectrometer from 400 to 4000 $cm^{-1}$. The surface morphology has been carried out using FESEM (Nova NanoSEM-450) and TEM (FEI MODEL-TECNAI TF 30 G2). Optical study was carried out by UV–Vis spectroscopy (UV-Visspectrophotometer-UV-2600) and photoluminescence spectroscopy (PL) technique at room temperature within the visible region range using 420 nm as the excitation wavelength on Edinburgh FS5 Spectro fluorometer. The I-V measurement has been carried out using an electrometer (Keysight, B2985A) under dark and illuminated conditions. Photo-current measurements were carried

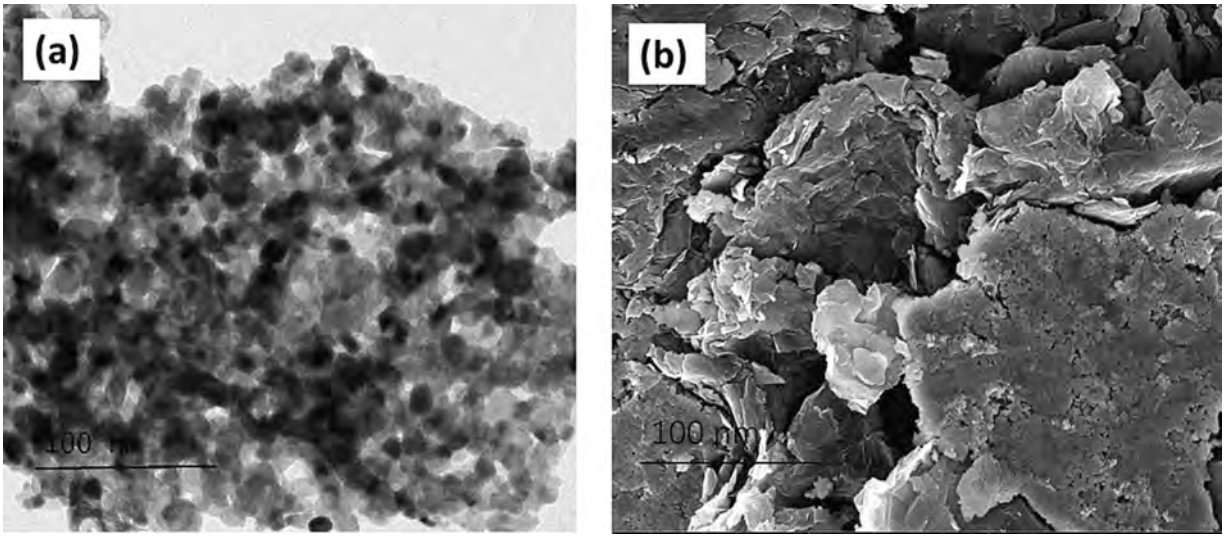


**Fig. 2.** FESEM micrographs for (a) Ag- $CoFe_2O_4$ nanoparticles and (b) GnPs doped Ag- $CoFe_2O_4$ nanocomposites.

out by using Keithley 6487 Pico ammeter/voltage source. Light dependent (visible light) impedance spectra have been carried out using an impedance analyzer (H20KI LCR meter (IM3570). Magnetic measurements were carried out using 7400 series, vibrating sample magnetometer (VSM) from Lake Shore Cryotronics at room temperature up to a maximum applied field of 15 kOe.

## 3. Results and discussion

### 3.1. Structural analysis

Structural characterization of the Ag-CFO nanoparticles and GnPs doped Ag-CFO nanocomposite has been carried out using XRD technique. The XRD spectra of Ag-CFO nanoparticles and GnPs doped Ag-CFO nanocomposite are represented in Fig. 1a and are cataloged with JCPDS No. 22-1086 using JCPDS software [37]. These standard peaks identified using the JCPDS reference card [22–1086], Ag-CFO peaks exhibit typical spinel structure of with Fd3m space group and are indexed to the (2 2 0), (3 1 1), (2 2 2), (4 0 0), (4 2 2), (5 1 1) and (4 4 0) with presence of Ag peaks. Presence of GnPs in CFO is confirmed from the peak around $\theta = 25^{o}$ corresponding to the most intense peak (0 0 2) of GnPs as shown in the Fig. 1. The obtained diffraction peaks do not display any shifting of peaks; however, owing to the incorporation of a carbon compound and existence of bio-extract in the Ag- CFO nanoparticles surface, the peak intensity of GnPs doped Ag- CFO nanocomposite is comparatively less [17]. It is noteworthy that the peak intensity of GnPs in the XRD pattern of nanocomposite is strongly observed which is possibly linked with the exfoliation of the graphene platelets in the resulting hybrid [38]. The lattice constants values obtained from the refined XRD data for Ag- CFO nanoparticles and GnPs doped Ag- CFO nanocomposite is found to be 8.92 Å and 8.47 Å, correspondingly, which agrees with JCPDS No. 22-1086 [37]. Using the well-known Scherrer's formula, the average crystallite size was determined to be 32.6 nm for Ag- CFO nanoparticles and 24 nm for GnPs doped Ag- CFO nanocomposite. This matches well with the particle size (in nm) estimated from the FESEM and TEM micrographs. The reduction of crystallite size in GnPs incorporated Ag- CFO is due to the presence of graphene which deforms the nanoferrite lattice structure affecting the particle size of the nanocomposite. The composite demonstrates enhanced structural stability in terms of particle size as compared to pure CFO which can be significant for long-term applications. To identify the functional group and vibrational mode, FT-IR pattern was scanned between 400 and 4000 $cm^{-1}$ regime and presented in Fig. 1b.

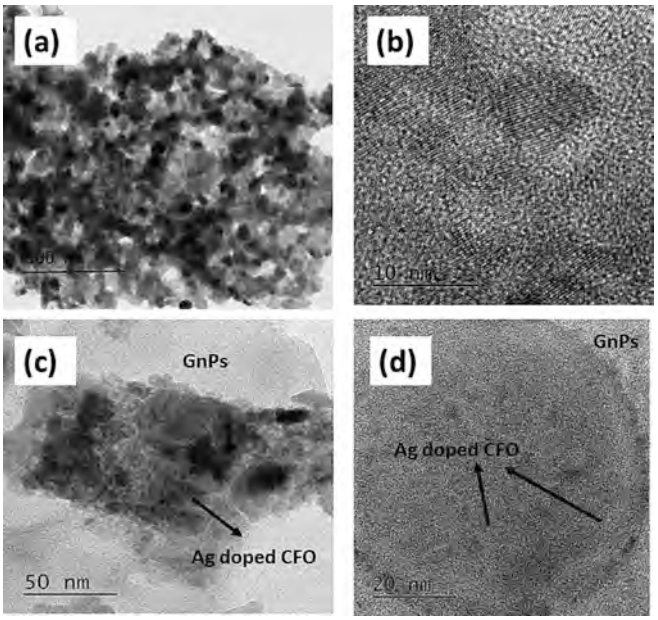


**Fig. 3.** (a) TEM micrograph of Ag doped $CoFe_2O_4$ nanoparticles, (b) HRTEM image of Ag doped $CoFe_2O_4$ nanoparticles; (c) TEM micrograph of Ag doped $CoFe_2O_4$ nanoparticles distributed as spherical particles in agglomerated form on the graphene sheets (d) the magnified HRTEM image of GnPs doped Ag-$CoFe_2O_4$ nanocomposites.

Ag- CFO nanoparticles display two spinel ferrites band around 583 $cm^{-1}$ and 411 $cm^{-1}$ signifying octahedral and tetrahedral voids. Formation of these bands is owed to the stretching vibrations in metal-oxygen bond ($Fe^{3+}$- $O^{2-}$). Also, existence of a characteristic peak at 1636 $cm^{-1}$ and 2934 $cm^{-1}$ is attributed to the C—H stretching and 2850 $cm^{-1}$ is O—H stretching. FT-IR spectrum of GnPs in Ag- CFO shows peaks of both GnPs and Ag- CFO (around 636 $cm^{-1}$) confirming the formation of GnPs -Ag-CFO. The presence of peaks at 1575 $cm^{-1}$ and 1086 $cm^{-1}$corresponds to the vibrational G-band suggesting in-plane bond stretching vibration of $sp^2$ bonded carbon atoms and C—O stretching vibration, respectively [39,40]. A peak is also seen at 1575 $cm^{-1}$ in the nanocomposite material which indicates that there is a small quantity of graphite in the graphene as a specific peak of the CC bond in its $sp^2$ structure [40].

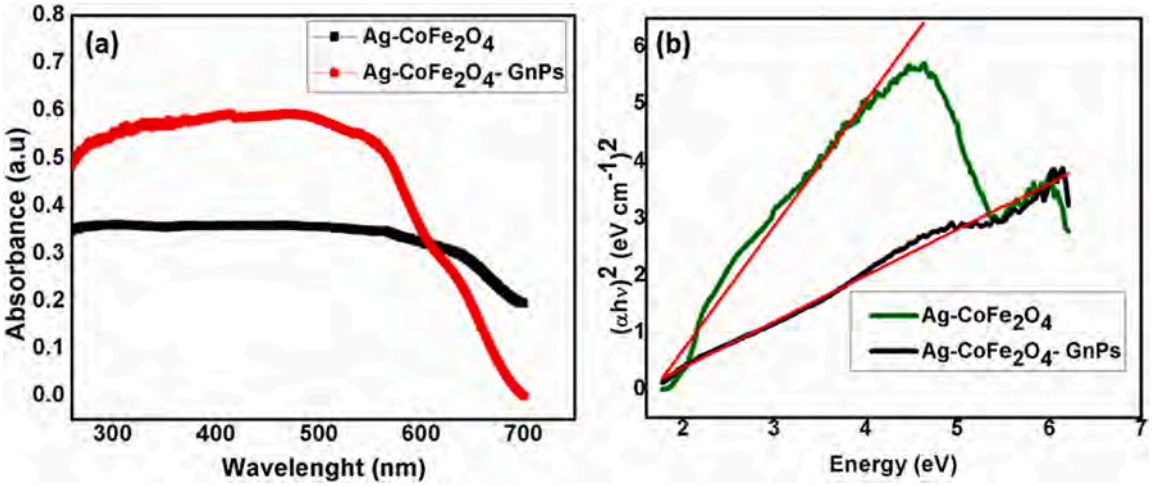


**Fig. 4.** (a) UV–visible absorption spectra and (b) corresponding Tauc plots of Ag doped $CoFe_2O_4$ nanoparticles and GnPs doped Ag- $CoFe_2O_4$ nanocomposites.

### 3.2. Morphological study

The surface morphology and the particle size for Ag- CFO nanoparticles and GnPs doped Ag- CFO nanocomposites and interaction of GnPs with the synthesized ferrite is analyzed by the obtained FESEM micrographs. From the FESEM image shown in Fig. 2a, the average diameter of the Ag- CFO nanoparticles are estimated to be about 40 nm and the particles seem to be agglomerated and clustered. In GnPs incorporated Ag- CFO, the ferrite nanoparticles seem to be distributed in the agglomerated form in the graphene sheets and is attributed to the $\pi - \pi$ interaction. It was expected that during the synthesis procedure the nano ferrite particles would grow on the surface of graphene sheets thereby weakening the $\pi - \pi$ interaction between the graphene particles but the FESEM micrographs shows that there is agglomeration of graphene sheets in the nanocomposite resembling a crumpled paper. The particles seen from the micrographs are homogenous with cluster size estimated in range of 25–30 nm. The microstructural study was further examined by TEM illustrated in Fig. 3.

The TEM images of Ag- CFO nanoparticles exhibited spherical and polyhedron shaped ferrite particles of nano-range order. The particle size lies between 36 nm to 40. From the micrographs it is observed that the Ag particles are agglomerated on the ferrite nanoparticles which may be the reason the particles appear bigger in size. However, the TEM image in Fig. 3c and d, it is observed that Ag- CFO nanoparticles are anchored on the nano GnPs surface in a impenetrable form and the average diameter of the particles lies between 20 and 28 nm. The obtained results are in agreement with the calculated values of XRD data. It is fascinating to observe that Ag particles and nano CFO are interlinked with the sheets of GnPs. This is evidenced from the micrographs even after the sonication process was conducted while preparing the samples in TEM grids signifying the presence of extraordinary adhesion between GnPs and Ag-CFO nanoparticles. To confirm the existence of Ag-CFO particles on GnPs surface, HRTEM image is captured and presented in Fig. 3d. The estimation of the interplanar (d) spacing obtained from the HRTEM images of the cubic spinel crystal of Ag- CFO nanoparticles CFO and GnPs doped Ag- CFO nanocomposites are valued to be 0.297 and 0.235 nm, respectively.

### 3.3. Optical studies

The optical absorbance spectrum of nano Ag- CFO particles and GnPs doped Ag-CFO hybrid have been performed using UV–vis spectrometer from 300 to 800 nm wavelength and presented in Fig. 4. The optical absorbance spectrum showed in Fig. 4(a) displays a shift in the absorption edge towards higher wavelength. This gradual shift in the

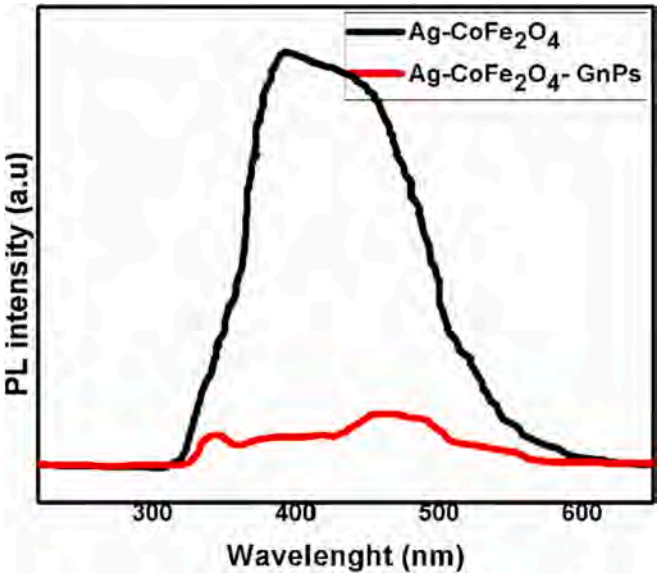


**Fig. 5.** PL spectra for (a) Ag doped $CoFe_2O_4$ nanoparticles and (b) GnPs doped Ag- $CoFe_2O_4$ nanocomposites.

absorption edge signifies a change in optical bandgap energy in the synthesized materials. Also, the possibility of nanocomposites to respond well to visible light paving way for application in photovoltaics as compared to Ag doped CFO [41]. The GnPs doped Ag- CFO nanocomposites are seen to display enhanced absorption capability and strong absorption intensity particularly when exposed to the visible light. The relation involving the optical bandgap energy ($E_g$) and absorption coefficient is represented by the Tauc's equation as:

$$(\alpha h\nu)^2 = h\nu - E_g$$

where, α denotes the absorption coefficient and $h$ represents the incident photon energy [42]. The plot of $(\alpha h\nu)^2$ vs. $h\nu$ is the Tauc plot illustrated in Fig. 4b.

It is calculated that from the intercept of the curve with x-axis, $E_g$ value for Ag- CFO nanoparticles is been found to 1.68 eV. However, by incorporation of GnPs, a change is observed in the band edge which is attributed to the successive energy in the sub-band gap formed due to significant interface and surface defects in the nano ferrite. This has caused the reduction in the band gap value to 1.44 eV in the hybrid material. The obtained results reveal that doping of GnPs in nanoferrite

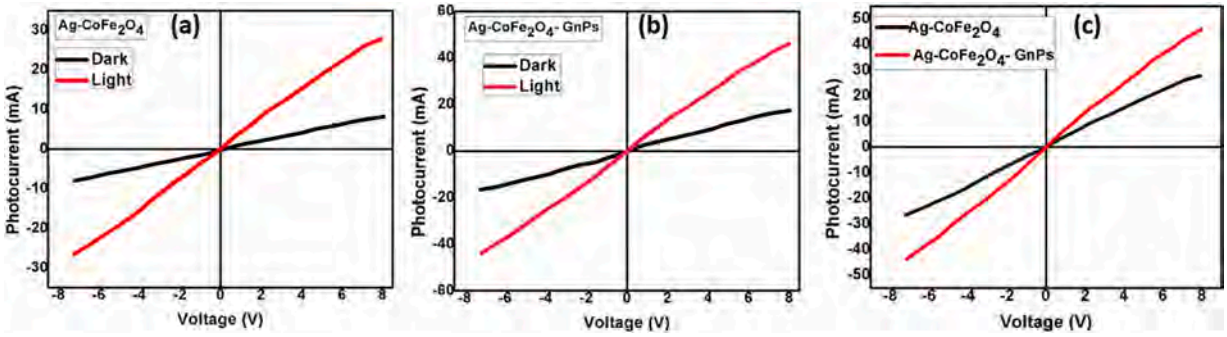


**Fig. 6.** Current-voltage (I-V) characteristics in light and dark mode for (a) Ag doped $CoFe_2O_4$ nanoparticles (b) GnPs doped Ag- $CoFe_2O_4$ nanocomposites (c) only light mode for Ag doped $CoFe_2O_4$ nanoparticles and GnPs doped Ag- $CoFe_2O_4$ nanocomposites.

can lessen the electron–hole recombination rate, thereby improving the photocatalytic activity of the GnPs-Ag-CFO nanocomposite. This also divulges that synthesized nanocomposite is semiconducting in nature [43]. The obtained band energy values are in consistent with the prior studies on transmission spectrum of ferrites. It a fact that graphene has exceptional value of electrical conductivity which favors the charge carriers transfer efficiently [27]. This in turn provides an extensive lifetime to the photogenerated electron–hole pairs. The effective transfer of charge carriers from the from Ag- CFO nanoferrites to graphene pallets and in case of GnPs incorporated Ag- CFO nanocomposite and the long-drawn-out recombination of electron–hole pairs were evidently shown by means of room temperature PL measurements. The PL spectra of nanoferrites and the hybrid recorded with a 340 nm excitation wavelength at room temperature are shown in Fig. 5. From the PL spectra it can be ascertained that the Ag- CFO spectrum displays a peak at 395 nm and is ascribed to the generation of holes and electrons in the valence and conduction bands due to the recombination [44].

Moreover, as revealed by PL spectra, a less intense PL spectrum peak (343 nm) akin to Ag- CFO is obtained for GnPs —Ag— CFO $_4$ nanocomposite. With incorporation of GnPs, the luminescence is substantially quenched owing to the interfacial charge transfer between the ferrites and graphene platelets [45]. This divulges the effective separation of the photogenerated charge carriers providing a suitable path for charge carriers that will control the recombination of the photogenerated electron–hole pairs which in turn increases their lifespan and photovoltaic performance [44].

### 3.4. Photo response study

The photocurrent (I) versus applied potential (V) curves of Ag- CFO nanoferrites and GnPs incorporated Ag- CFO nanocomposite is shown in Fig. 6. Upon illumination Ag- CFO nanoferrites displayed photo excitation, accelerating the growth of electron–hole pairs. The photocurrent density for nanoferrites, is comparatively less than GnPs doped ferrite which may be because of the absorption of radiation under illumination. This may excite the electrons to generate photocurrent owing to the Schottky barrier at the interface of the metal and the ferrite and is responsible for the charge transfer mechanism [46]. When GnPs are incorporated in the Ag- CFO nanoferrites, the synthesized nanocomposites are also able to capture the photo-induced electrons as the excited electrons that get generated in the nanoferrite structure are transferred to the graphene platelets which separates the photogenerated charge carriers much efficiently. This is because of the large surface area and superior conductivity of GnPS and it is also known that GnPs facilitates the conductivity of the electrons owing to the excellent charge transport properties [27,46–48]. This promotes the charge separation and transportation process in the nanocomposites and enhances the lifetime of the photo-generated electrons as it is capable of separation of photogenerated electrons and holes. Hence, the photocurrent values for GnPs doped nanoferrites gets alleviated indicating the separation and transfer of the electron-hole pairs.

### 3.5. Light dependent impedance study

EIS is basically a technique used to analyze the contribution of intrinsic factors (grain-boundaries, grain) and extrinsic factors (interface properties) responsible for the electrical and dielectric study [49]. The room temperature CIS of the synthesized nano ferrites and nanocomposites is conceded in the frequency range of $10^2$ Hz to 1 MHz.

The impedance analysis has been carried out in the dark and under

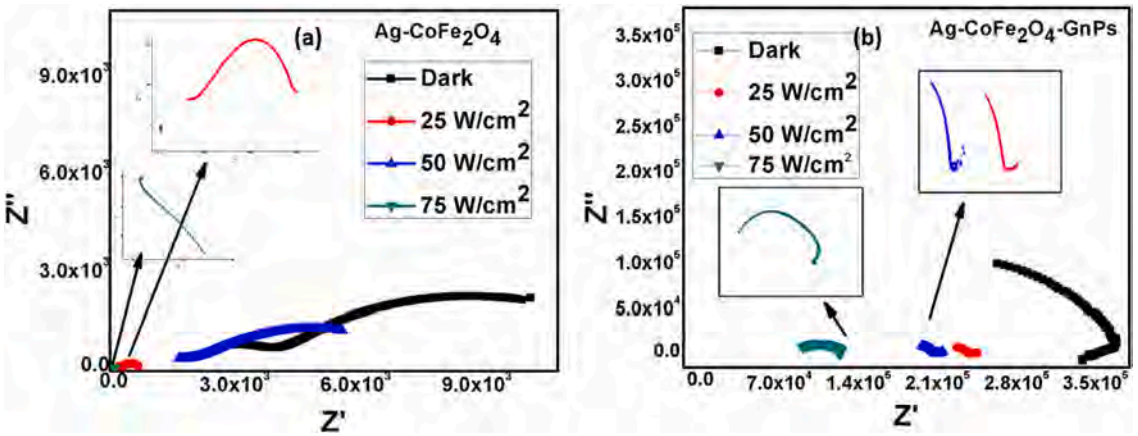


**Fig. 7.** Nyquist plot of impedance of (a) Ag doped $CoFe_2O_4$ nanoparticles (b) GnPs doped Ag- $CoFe_2O_4$ nanocomposites in the dark condition (light off) and under continuous illumination (light on) with varying light intensities from 0 to 100 W/$m^2$.

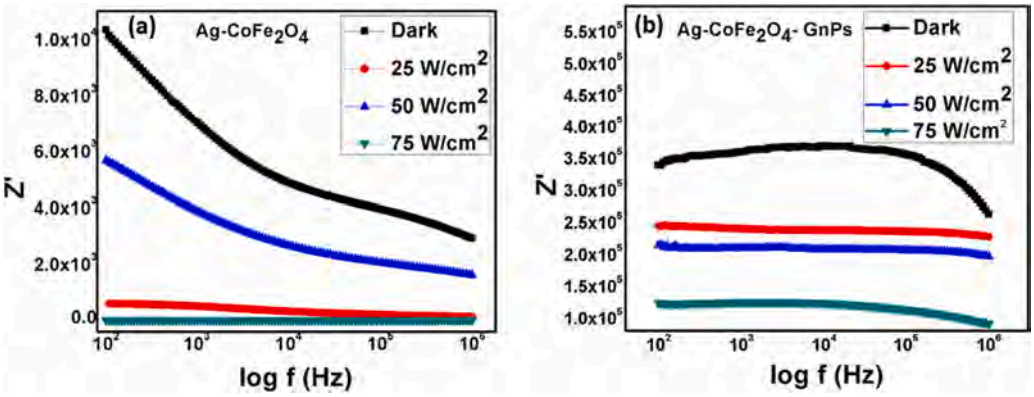


**Fig. 8.** Room temperature variation of real part of impedance (Z′) with frequency for (a) Ag doped $CoFe_2O_4$ nanoparticles (b) GnPs doped Ag- $CoFe_2O_4$ nanocomposites in the dark and under illumination with varying light intensities from 0 to 100 W/m$^2$.

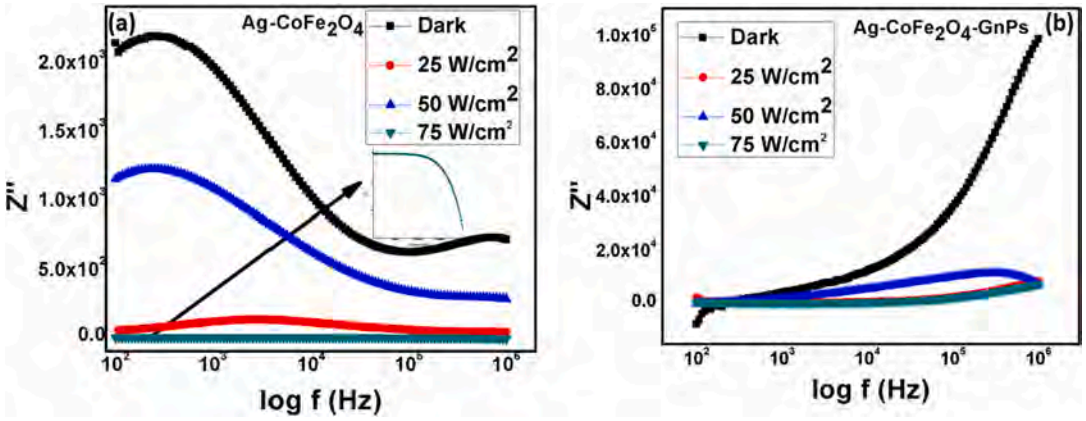


**Fig. 9.** Room temperature variation of imaginary part of impedance (Z″) with frequency for (a) Ag doped $CoFe_2O_4$ nanoparticles (b) GnPs doped Ag- $CoFe_2O_4$ nanocomposites in the dark and under illumination with varying light intensities from 0 to 100 W/m$^2$.

illumination at room temperature. The measurements under illumination were performed with a with varying light intensities from 0 to 100 W/m$^2$. To achieve *light intensities* of 25, 50 and 75 W/m$^2$, the distance between the light source and sample was *varied*. Also, the frequency domain in the Nyquist plot of impedance can be processed easily owing to the recombination process that dominates the dark and the photocurrent. The Nyquist plots shown in Fig. 7 for the synthesized materials display two semicircle arcs indicating the occurrence of relaxation phenomena of two different kinds. The observed semicircular arcs seem to be de-centered from the axis which implies the occurrence of non-Debye type of relaxation mechanism. Also, the decentralization of the arcs approves the occurrence of a single electrical conduction phenomenon. The diameter of the semicircular arc is extremely dependent on the intensity of light and seems to be gradually decreasing with increasing light intensity [49]. This gradual reduction is ascribed to the internal charge transfer occurring between the grain and the interface. Under illumination, the nyquist plot seems to be decreasing which is owed to the production of excitons occurring within the system and thereafter it starts to diffuse towards the interface. Also, a charge separation takes place while the excitons change their states. This happens

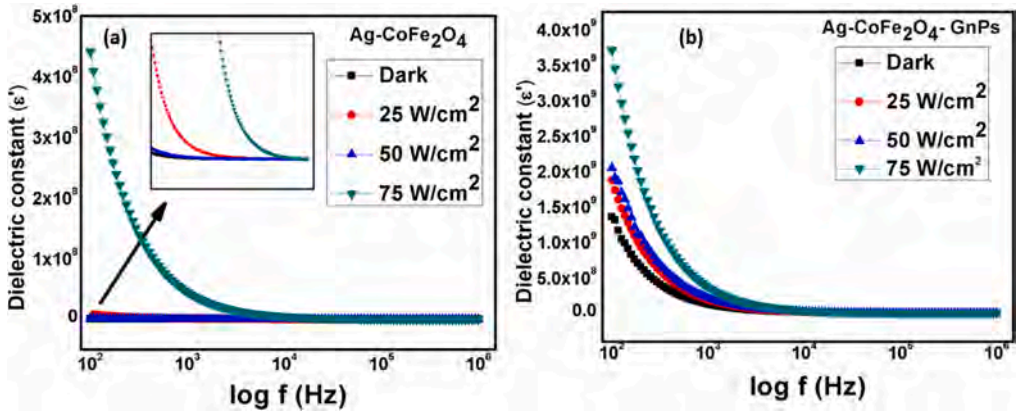


**Fig. 10.** Real part of permittivity (ε') as a function of frequency in the dark and under illumination with varying light intensities from 0 to 100 W/m$^2$ for (a) Ag doped $CoFe_2O_4$ nanoparticles (b) GnPs doped Ag- $CoFe_2O_4$ nanocomposites.

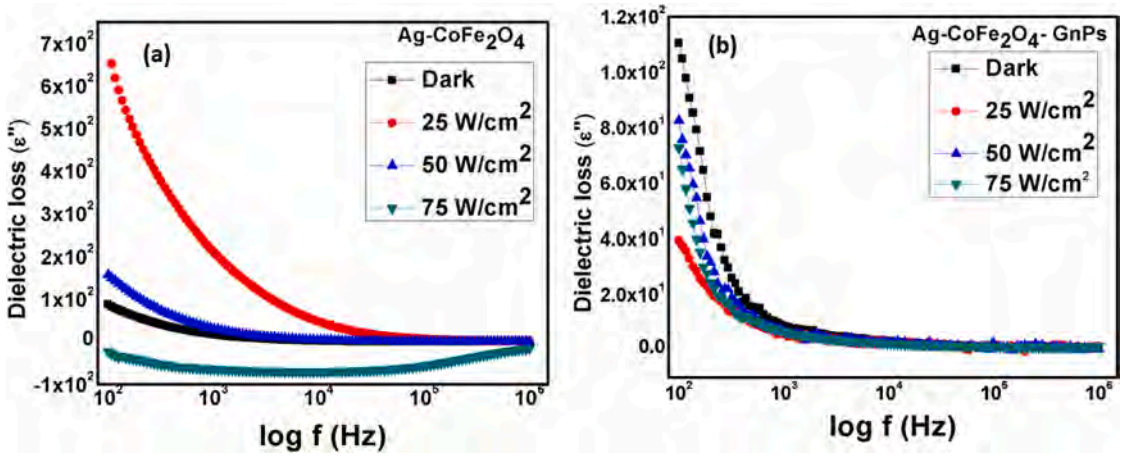


**Fig. 11.** Real part of permittivity (ε') as a function of frequency in the dark and under illumination with varying light intensities from 0 to 100 W/m$^2$ for (a) Ag doped $CoFe_2O_4$ nanoparticles (b) GnPs doped Ag- $CoFe_2O_4$ nanocomposites.

at the interface through internal transfer of charges and owing to this, the free charge carriers are produced in the system leading to the diminution in the diameter of the semicircles.

Fig. 8a represents the room temperature variation of Z′ with frequency. An elevation in Z′ values is seen at lower range of frequency which gradually decreases with increasing frequency. At higher value of frequency, a serious decay in Z′ is seen that is attributed to the presence of the space-charge region. Under illumination, in the lower frequency range, the frequency vs Z′ plots seem to be dependent on the intensity of the light and with the increase in intensity of the light, the curves seem to be decreasing. This may be attributed to the charge carriers flowing in the material. This discrepancy in Z′ implies the light dependent behavior which affects the resistance of the synthesized material [50].

Z″ as a function of frequency for the materials at room temperature in dark and with varying light intensities is presented in Fig. 9. With increase in frequency, Z″ gradually starts to decrease. The plots exhibit wide and less intensity peaks approaching towards the higher side of frequency suggesting the occurrence of a relaxation phenomenon [50]. Debye-type relaxation peak where Z″ curves increase initially and then decreases with increase in frequency is observed which indicates the presence of space charges as the electrical nature of space charges depends on the frequency. It is also divulged that height of the peaks decreases with upsurge in light intensity. This is indicative of a light dependent dielectric relaxation phenomenon.

### 3.6. Dielectric studies

The real part of permittivity (ε') vs. frequency for the synthesized nanoparticles and the nanocomposites with varying light intensities is shown in Fig. 10. It is divulged from the plot that ε' acts inversely in accordance to the change in frequency which actually is a characteristic feature exhibited by all dielectric and/or ferroelectric materials. This is explicated on the basis of Maxwell Wagner type interfacial polarization in agreement with the Koop's phenomenological theory [51]. The motive of the observed behavior is owed to the free charges which build up owing to the formation of defects. These defects occur due to the presence of oxygen vacancies during the synthesis of the material intensifying the space charges on exposure to the external applied electric field. At lower frequency, the charges acquire enough time to cover greater path in the sample, causing a huge electronic polarization, hence a greater value of ε' is obtained. The incorporation of graphene in the nanocomposite has resulted in improved electrical conductivity as compared to CFO and, this could be advantageous for electronic applications. With increase in the value of frequency, the charge carriers lag to respond to the changing applied external field and this results in a reduced polarizability in the material.

Fig. 11 divulges the imaginary part of permittivity (ε'') of Ag- CFO nanoparticles and Ag-CFO-GnPs nanocomposites at varying light intensities as a function of frequency. The plots display an increase in ε'' values when temperature increases. Both ε' and ε″ seem to follow the same change and are able to control the dissipation of charge and energy. Increase in ε'' is ascribed to the conduction mechanism that possibly comprises of transferring ions to greater distances. It is in fact that with increasing temperature, ac conductivity rises ensuing an increase in conduction and dipole loss [49–51]. This results in increase of ε'' value. When Ag-CFO is blended with GnPs enhanced dielectric values are obtained owing to the larger conductivity values and superior aspect ratio of GnPs that builds up a conducting network in the Ag-CFO matrix. This might be also because of the GnPs that act as parallel plate capacitor among which the polarization effect by dipoles formation in ferrite matrix improves the charge storage capacity by increasing the charge contents [50]. The ε' and ε'' for nanocomposites is clearly better than the nanoferrites representing the anchoring of GnPs in the ferrite improves the dielectric behavior. Nevertheless, the loss obtained is significantly less suggesting a negligible contribution to absorption of the EM noise. It can be expected that this could obviously overpower EM noise at even higher frequency values than that mentioned here. In addition, the TEM micrographs reveal the porosity of the as-synthesized nanocomposites which helps in reducing the eddy current loss in high frequency magnetic materials. Hence, these materials find suitability in high frequency-based devices.

### 3.7. Magnetic analysis

The magnetic hysteresis (M-H) curve for Ag doped CFO nanoparticles and GnPs doped Ag- CFO nanocomposites were obtained by applying the magnetic field upto 15 kOe. It reveals that the Ag doped CFO nanoparticles exhibit a long-range ferromagnetic ordering. However, the coercivity value obtained is minimal which is owed to the smaller grain size of the nanoparticles. In this case, the size of the nanoparticles is insufficient to overcome the thermal energy for which the energy barrier becomes less. Hence, the material has higher value of magnetism but lesser coercivity. On incorporation of GnPs, ferromagnetic behavior is observed [52]. The saturation magnetization ($M_s$) value was around 40 kOe for Ag doped CFO nanoparticles which on incorporation of GnPs reduced to 2.8 kOe. This is owed to the nonmagnetic nature of GnPs, however, the ferromagnetism in GnPs doped Ag- CFO nanocomposites is originated from the hybridization of $p_z$ orbital of GnPs and d orbital of Ag-CFO. This alters the electronic configuration of the nanocomposites resulting in ferromagnetic interaction. The composites exhibit improved

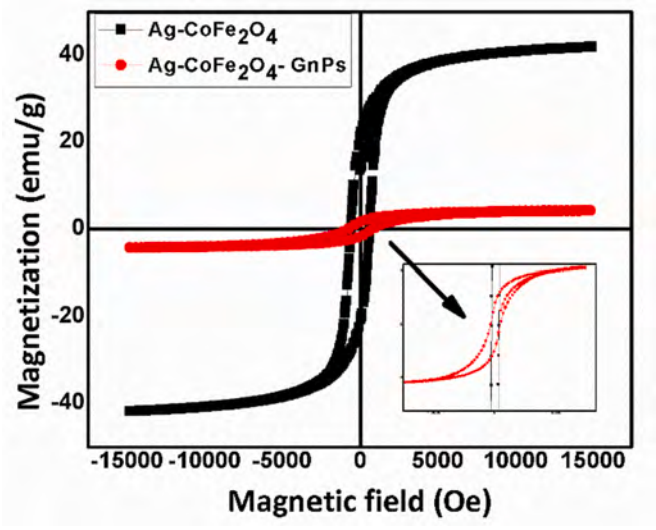


**Fig. 12.** Magnetic hysteresis curve for (a) Ag doped $CoFe_2O_4$ nanoparticles and (b) GnPs doped Ag- $CoFe_2O_4$ nanocomposites.

magnetization such as $M_s$ as compared to pure CFO which can be considered essential for magnetic applications (Fig. 12).

## 4. Conclusion

GnPs anchored into nano Ag-$CoFe_2O_4$ hybrid was successfully synthesized using a simple solvothermal method using green synthesis method by okra plant extract. From the XRD data, the average crystallite size was determined to be 32.6 nm for Ag- CFO nanoparticles and 24 nm for GnPs doped Ag- CFO nanocomposite which matches well with the particle size (in nm) estimated from the FESEM and TEM micrographs. The optical bandgap energy ($E_g$) value for Ag- CFO nanoparticles is found to be 1.68 eV which on incorporation of GnPs reduced to 1.44 eV, thereby improving the photocatalytic activity of the GnPs-Ag-CFO nanocomposite. The electrical and dielectric properties were evaluated at light intensities light intensities from 0 to 100 W/$m^2$ and frequencies ranging from 100 Hz to 1 MHz as a function of composition. Under illumination, Debye-type relaxation peak is observed where Z″ curves increase initially and then decreases with increase in frequency. Nyquist plot seems to be decreasing which is owed to the production of excitons occurring within the system and thereafter it starts to diffuse towards the interface. The ε' and ε'' for nanocomposites is clearly better than the nanoferrites representing the anchoring of GnPs in the ferrite improves the dielectric behavior. The saturation magnetization ($M_s$) value was around 40 kOe for Ag doped CFO nanoparticles which on incorporation of GnPs reduced to 2.8 kOe; additionally, this alters the electronic configuration of the nanocomposites resulting in ferromagnetic interaction.

## CRediT authorship contribution statement

Krutika L. Routray: Methodology, Synthesis and Data collection Data curation, Writing- Original draft preparation, revision

Sunirmal Saha: Conceptualization, Supervision, Reviewing and Editing, revision

## Declaration of competing interest

Dr. Sunirmal Saha reports was provided by C V Raman Global University. Dr. Sunirmal Saha reports a relationship with C V Raman Global University that includes: employment.

## Data availability

Data will be made available on request.

## Refrences

[1] D.H.K. Reddy, Y.S. Yun, Spinel ferrite magnetic adsorbents: alternative future materials for water purification? Coord. Chem. Rev. 315 (2016) 90–111.
[2] K.K. Kefeni, B.B. Mamba, Photocatalytic application of spinel ferrite nanoparticles and nanocomposites in wastewater treatment, SM&T 23 (2020), e00140.
[3] S. Chakrabarty, M. Pal, A. Dutta, Yttrium doped cobalt ferrite nanoparticles: study of dielectric relaxation and charge carrier dynamics, Ceram. Int. 44 (12) (2018) 14652–14659.
[4] G. Asab, E.A. Zereffa, T. Abdo Seghne, Synthesis of silica-coated Fe3O4 nanoparticles by microemulsion method: Characterization and evaluation of antimicrobial activity, Int. J. Biomater. 4783612 (2020) 1–11.
[5] G. Baldi, D. Bonacchi, C. Innocenti, G. Lorenzi, C. Sangregorio, Cobalt ferrite nanoparticles: the control of the particle size and surface state and their effects on magnetic properties, J. Magn. Magn. 311 (1) (2007) 10–16.
[6] G. Allaedini, S.M. Tasirin, P. Aminayi, Magnetic properties of cobalt ferrite synthesized by hydrothermal method, Int. Nano Lett. 5 (2015) 183–186.
[7] P. Thakur, D. Chahar, S. Taneja, N. Bhalla, A. Thakur, A review on MnZn ferrites: Synthesis, characterization and applications, Ceramics international 46 (10) (2020) 15740–15763.
[8] T.E. Quickel, V.H. Le, T. Brezesinski, S.H. Tolbert, On the correlation between nanoscale structure and magnetic properties in ordered mesoporous cobalt ferrite (CoFe2O4) thin films, Nano Lett. 10 (8) (2010) 2982–2988.
[9] Y. Kumar, A. Sharma, P.M. Shirage, Impact of different morphologies of CoFe2O4 nanoparticles for tuning of structural, optical and magnetic properties, J. Alloys Compd. 778 (2019) 398–409.
[10] L.J. Sanchez, Dielectric and Complex Impedance Properties of Tetravalent Hafnium (HF 4+) Integrated Cobalt Ferrite, The University of Texas at El Paso, 2013.
[11] M. Amiri, M. Salavati-Niasari, A. Akbari, Magnetic nanocarriers: evolution of spinel ferrites for medical applications, Adv. Colloid Interface Sci. 265 (2019) 29–44.
[12] F. Sharifianjazi, M. Moradi, N. Parvin, A. Nemati, A.J. Rad, N. Sheysi, A. Abouchenari, A. Mohammadi, S. Karbasi, Z. Ahmadi, A. Esmaeilkhanian, Magnetic CoFe2O4 nanoparticles doped with metal ions: a review, Ceram. Int. 46(11) (2020) 18391–18,412.
[13] R. Sharma, S. Singhal, Structural, magnetic and electrical properties of zinc doped nickel ferrite and their application in photo catalytic degradation of methylene blue, Phys. B: Condens. 414 (2013) 83–90.
[14] M. Pooladi, H. Shokrollahi, S.A.N.H. Lavasani, H. Yang, Investigation of the structural, magnetic and dielectric properties of Mn-doped Bi2Fe4O9 produced by reverse chemical co-precipitation, Mater. Chem. Phys. 229 (2019) 39–48.
[15] K.L. Routray, D. Sanyal, D. Behera, Dielectric, magnetic, ferroelectric, and Mossbauer properties of bismuth substituted nanosized cobalt ferrites through glycine nitrate synthesis method, J. Appl. Phys. 122 (22) (2017).
[16] S. Karmakar, K.L. Routray, B. Panda, B. Sahoo, D. Behera, Construction of core@ shell nanostructured NiFe2O4@ TiO2 ferrite NAND logic gate using fluorescence quenching mechanism for TiO2 sensing, J. Alloys Compd. 765 (2018) 527–537.
[17] K.L. Routray, S. Saha, D. Behera, Insight into the anomalous electrical behavior, dielectric and magnetic study of Ag-Doped CoFe 2 O 4 synthesized by Okra extract-assisted green synthesis, J. Electron. Mater. 49 (2020) 7244–7258.
[18] P. Mahajan, A. Sharma, B. Kaur, N. Goyal, S. Gautam, Green synthesized (*Ocimum sanctum* and *Allium sativum*) Ag-doped cobalt ferrite nanoparticles for antibacterial application, J. Vac. Sci. 161 (2019) 389–397.
[19] M.K. Satheeshkumar, E. Ranjith Kumar, C.H. Srinivas, N. Suriyanarayanan, M. Deepty, C.L. Prajapat, T.V. Chandrasekhar Rao, D.L. Sastry, Study of structural, morphological and magnetic properties of Ag substituted cobalt ferrite nanoparticles prepared by honey assisted combustion method and evaluation of their antibacterial activity, J. Magn. Magn. 469 (2019) 691–697.
[20] M. Kaiser, Effect of silver nanoparticles on properties of cobalt ferrites, J. Electron. Mater. 49 (8) (2020) 5053–5063.
[21] A. Lagashetty, A. Pattar, S. Ganiger, Synthesis and characterization of Ag doped cobalt ferrite nanocomposite, Int J Nano Dimens. 10 (3) (2019) 291–296.
[22] R. Amini, G. Nabiyouni, S. Jarollahi, Removal of azo dyes pollutants: photocatalyst and magnetic investigation of iron oxide-zinc sulfide nanocomposites, J. Nanostructure 11 (1) (2021) 95–104.
[23] M. Dong, H. Zhang, L. Tzounis, G. Santagiuliana, E. Bilotti, D.G. Papageorgiou, Multifunctional epoxy nanocomposites reinforced by two-dimensional materials: a review, Carbon 185 (2021) 57–81.
[24] W. Cai, B.B. Wang, X. Wang, Y.L. Zhu, Z.X. Li, Z.M. Xu, L. Song, W.Z. Hu, Y. Hu, Recent progress in two-dimensional nanomaterials following graphene for improving fire safety of polymer (nano) composites, CJPS 39 (8) (2021) 935–956.
[25] S. Ramezani, M.H. Mashhadizadeh, R. Jahani, M. Kamali, Carbon nanotube grafted pyridinuim compound as a neutral ion-carrier of carbon paste electrode for sub-nanomolar simultaneous monitoring of Cu (II) and Hg (II), Int. J. Environ. Anal. Chem. 1–24 (2023).
[26] F. Meng, H. Wang, F. Huang, Y. Guo, Z. Wang, D. Hui, Z. Zhou, Graphene-based microwave absorbing composites: a review and prospective, Compos. B. Eng. 137 (2018) 260–277.
[27] M. Kumar, H.S. Dosanjh, J. Singh, K. Monir, H. Singh, Review on magnetic nanoferrites and their composites as alternatives in waste water treatment:

synthesis, modifications and applications, Environ. Sci. Water Res. Technol. 6 (3) (2020) 491–514.
[28] A.M.A. Henaish, M.M. Ali, D.E. Refaay, I.A. Weinstein, O.M. Hemeda, Synthesis, electric and magnetic characterization of nickel ferrite/PANI nano-composite prepared by flash auto combustion method, J. Inorg. Organomet. Polym. Mater. 31 (2021) 731–740.
[29] S.A. Saafan, M.K. El-Nimr, M.M. Hussein, M.K. Omar, FTIR, DC, and AC electrical measurements of Mg Zn Nano-ferrites and their composites with polybenzoxazine, Appl. Phys. A. 127 (2021) 1–14.
[30] Y. Kumar, S. Pradhan, S. Pramanik, R. Bandyopadhyay, D.K. Das, P. Pramanik, Efficient electrochemical detection of guanine, uric acid and their mixture by composite of nano-particles of lanthanides ortho-ferrite XFeO3 (X = La, Gd, Pr, Dy, Sm, Ce and Tb), J. Electroanal. Chem. 830 (2018) 95–105.
[31] S.F. Adil, M.E. Assal, M. Khan, A. Al-Warthan, M.R.H. Siddiqui, L.M. Liz-Marzán, Biogenic synthesis of metallic nanoparticles and prospects towards green chemistry, Dalton Transactions 44 (21) (2015) 9709–9717.
[32] F. Benakashani, A. Allafchian, S.A.H. Jalali, Green synthesis, characterization and antibacterial activity of silver nanoparticles from root extract of *Lepidium draba* weed, GCLR 10 (4) (2017) 324–330.
[33] K.L. Routray, S. Saha, D. Behera, Green synthesis approach for nano sized CoFe2O4 through *aloe vera* mediated sol-gel auto combustion method for high frequency devices, Mater. Chem. Phys. 224 (2019) 29–35.
[34] M. Behzadi, S. Jarollahi, M. Ahsani Irvani, D. Ghanbari, Green Synthesis and Antibacterial Activity of Silver Nanoparticles Using *Dracocephalum Moldavica* Leaves Extract, J. Nanostructure 12 (4) (2022) 1059–1066.
[35] S. Ahmadian-Fard-Fini, M. Salavati-Niasari, D. Ghanbari, Hydrothermal green synthesis of magnetic Fe3O4-carbon dots by lemon and grape fruit extracts and as a photoluminescence sensor for detecting of *E. coli* bacteria, Spectrochim. Acta A Mol. Biomol. Spectrosc. 203 (2018) 481–493.
[36] S. Ahmadian-Fard-Fini, D. Ghanbari, M. Salavati-Niasari, Photoluminescence carbon dot as a sensor for detecting of *Pseudomonas aeruginosa* bacteria: hydrothermal synthesis of magnetic hollow NiFe2O4-carbon dots nanocomposite material, Compos. B. Eng. 161 (2019) 564–577.
[37] E.J. Choi, Y. Ahn, S. Kim, D.H. An, K.U. Kang, B.-G. Lee, K.S. Baek, H.N. Oak, Superparamagnetic relaxation in $CoFe_2O_4$ nanoparticles, J. Magn. Magn. Mater. 262 (2003).
[38] C.I. Idumah, A. Hassan, Characterization and preparation of conductive exfoliated graphene nanoplatelets kenaf fibre hybrid polypropylene composites, Synth. Met. 212 (2016) 91–104.
[39] V. Ţucureanu, A. Matei, A.M. Avram, FTIR spectroscopy for carbon family study, Crit. Rev. Anal. Chem. 46 (6) (2016) 502–520.
[40] R. Medhi, M.D. Marquez, T.R. Lee, Visible-light-active doped metal oxide nanoparticles: review of their synthesis, properties, and applications, ACS Appl. Nano Mater. 3 (7) (2020) 6156–6185.
[41] N.A. Bakr, Z.T. Khodair, S.M. Hassan, Effect of substrate temperature on structural and optical properties of Cu2ZnSnS4 (CZTS) films prepared by chemical spray pyrolysis method, Res. J. Chem. Sci. 2231 (2015) 606×.
[42] S.B. Aziz, M.A. Rasheed, H.M. Ahmed, Synthesis of polymer nanocomposites based on [methyl cellulose](1− x):(CuS) x (0.02 M ≤ x ≤ 0.08 M) with desired optical band gaps, Polym. J. 9 (6) (2017) 194.
[43] C. Li, H. Che, P. Huo, Y. Yan, C. Liu, H. Dong, Confinement of ultrasmall CoFe2O4 nanoparticles in hierarchical ZnIn2S4 microspheres with enhanced interfacial charge separation for photocatalytic H2 evolution, J. Colloid Interface Sci. 581 (2021) 764–773.
[44] J. Lee, K. Kim, W.I. Park, B.H. Kim, J.H. Park, T.H. Kim, S. Bong, C.H. Kim, G. Chae, M. Jun, Y. Hwang, Uniform graphene quantum dots patterned from self-assembled silica nanodots, Nano Lett. 12 (12) (2012) 6078–6083.
[45] K.K. Das, S. Patnaik, S. Mansingh, A. Behera, A. Mohanty, C. Acharya, K.M. Parida, Enhanced photocatalytic activities of polypyrrole sensitized zinc ferrite/graphitic carbon nitride nn heterojunction towards ciprofloxacin degradation, hydrogen evolution and antibacterial studies, J. Colloid Interface Sci. 561 (2020) 551–567.
[46] S. Hajra, S. Sahoo, R. Das, R.N.P. Choudhary, Structural, dielectric and impedance characteristics of (Bi0. 5Na0. 5) TiO3-BaTiO3 electronic system, J. Alloys Compd. 750 (2018) 507–514.
[47] A. Kiani, G. Nabiyouni, S. Masoumi, D. Ghanbari, A novel magnetic MgFe2O4–MgTiO3 perovskite nanocomposite: rapid photo-degradation of toxic dyes under visible irradiation, Compos. B. Eng. 175 (2019), 107080.
[48] N. Eskandari, G. Nabiyouni, S. Masoumi, D. Ghanbari, Preparation of a new magnetic and photo-catalyst CoFe2O4–SrTiO3 perovskite nanocomposite for photo-degradation of toxic dyes under short time visible irradiation, Compos. B. Eng. 176 (2019), 107343.
[49] G. Garcia-Belmonte, P.P. Boix, J. Bisquert, M. Sessolo, H.J. Bolink, Simultaneous determination of carrier lifetime and electron density-of-states in P3HT: PCBM organic solar cells under illumination by impedance spectroscopy, Sol. Energy Mater Sol. Cells. 94 (2) (2010) 366–375.
[50] M. Hashim, S. Kumar, S. Ali, B.H. Koo, H. Chung, R. Kumar, Structural, magnetic and electrical properties of Al3+ substituted Ni—Zn ferrite nanoparticles, J. Alloys Compd. 511 (1) (2012) 107–114.
[51] R.H. Kodama, Magnetic nanoparticles, J. Magn. Magn. 200 (1–3) (1999) 359–372.
[52] O.S. Yakovenko, L.Y. Matzui, L.L. Vovchenko, A.V. Trukhanov, I.S. Kazakevich, S. V. Trukhanov, Y.I. Prylutskyy, U. Ritter, Magnetic anisotropy of the graphite nanoplatelet–epoxy and MWCNT–epoxy composites with aligned barium ferrite filler, Journal of Materials Science 52 (2017) 5345–5358.